Future sea-level rise projections for tide gauge locations in South Asia

Environmental Research Communications

PAPER

Future sea-level rise projections for tide gauge locations in South Asia

Benjamin J Harrison[1], **Joseph D Daron**[1,2], **Matthew D Palmer**[1,2] and **Jennifer H Weeks**[1]

[1] Met Office, FitzRoy Road, Exeter, EX1 3 PB, United Kingdom
[2] University of Bristol, Bristol, BS8 1UH, United Kingdom

E-mail: benjamin.harrison@metoffice.gov.uk

Keywords: climate change, terrestrial water storage, regional sea-level change, tide gauge observations

Supplementary material for this article is available online

OPEN ACCESS

RECEIVED
3 July 2021

REVISED
20 September 2021

ACCEPTED FOR PUBLICATION
11 October 2021

PUBLISHED
10 November 2021

Abstract

Local projections of future sea-level change are important for understanding climate change risks and informing coastal management decisions. Reliable and relevant coastal risk information is especially important in South Asia, where large populations live in low-lying areas and are at risk from coastal inundation. We present a new set of local sea-level projections for selected tide gauge locations in South Asia. The projections are used to explore the drivers of spatial variations in sea-level change for South Asia over the 21st century under the RCP2.6 and RCP8.5 scenarios. Global sea-level rise for 2081–2100 is projected to be 0.39 m (0.26–0.58 m) and 0.65 m (0.47 m–0.93m) for RCP2.6 and RCP8.5 respectively. Local sea-level rise projections for the same period vary spatially over the South Asia region, with local sea-level rise in excess of projected global sea-level rise in the equatorial Indian Ocean but less than projected global sea-level rise for the northern Arabian Sea and northern Bay of Bengal. Local sea-level rise for 2081–2100 is projected to be 0.44 m (0.29–0.67 m) and 0.72 m (0.51–1.06 m) at Gan II (Maldives) under RCP2.6 and RCP8.5 respectively, whereas for Diamond Harbour (West Bengal) the corresponding changes are 0.32 m (0.19–0.51 m) and 0.57 m (0.39–0.85m). We find that the sterodynamic contribution is generally the leading driver of change at any single location, with future groundwater extraction over the sub-continent landmass the main driver of spatial variations in sea-level across the region. The new localised projections quantify and enhance understanding of future sea-level rise in South Asia, with the potential to feed into decisions for coastal planning by local communities, government, and industry.

1. Introduction

Sea-level rise is of paramount concern in coastal regions of South Asia, where large populations are vulnerable and exposed to flooding from coastal inundation and surge events (Brecht *et al* 2012, Hijioka *et al* 2014). Reliable projections of sea-level change at spatial and temporal scales of relevance to climate change adaptation and investment decisions are required in order to ensure risks are understood and managed. However, the precise nature of sea-level information required depends on the decision context and levels of uncertainty tolerance (Hinkel *et al* 2019).

Sea-level change is known to vary regionally, differing in the magnitude and rate of change, and in some locations the sign of change (Oppenheimer *et al* 2019). Spatial variations in sea-level change can arise from differences in the relative contributions from local ocean dynamic processes (i.e. ocean circulation and density changes) as well as changes in Earth's gravity, rotation, and viscoelastic solid-earth deformation that arise from the redistribution of mass from the continents to the oceans (e.g. through melting of ice sheets, glaciers and groundwater depletion) (Mitrovica *et al* 2001, Stammer *et al* 2013, Slangen *et al* 2014). Understanding and quantifying different contributions, or 'fingerprints', of regional and local sea-level change is essential for making more robust use of climate model datasets and providing projections at sub-global scales (Tamisiea and Mitrovica 2011).

Regional sea-level projections have been produced using knowledge of the different contributions applied to the outputs of coupled ocean-atmosphere climate model simulations, such as those produced through the fifth phase of the Coupled Model Intercomparison Project (CMIP5) (e.g. Slangen *et al* 2014, Palmer *et al* 2020). Most studies to date in South Asia have relied on global or basin-scale (e.g. Bay of Bengal) sea-level projections (Kay *et al* 2015, Jisan *et al* 2018, Rahman *et al* 2019), such as those provided in the fifth assessment report of the Intergovernmental Panel on Climate Change (IPCC) (Church *et al* 2013). For example, studies assessing coastal risks in Pakistan have relied either on global estimates of sea-level change provided by IPCC reports, or extrapolations of observed changes from a single tide gauge location (Karachi) (see Weeks and Harrison 2020). As part of a recent assessment of climate change over the Indian region, Swapna *et al* (2020) state that sea-level rise in the Indian Ocean is dominated by thermal expansion with the thermosteric component likely to contribute about 20 to 30 cm of sea-level rise along the Indian coast by the end of the twenty-first century. However, the study does not consider all important regional contributions and only uses a single greenhouse gas concentration scenario (RCP4.5), thereby only capturing part of the uncertainty space.

In this paper, we investigate future sea-level change along the coasts of South Asia. We focus on the change in local time mean sea-level relative to the local solid surface, following the terminology set out in Gregory *et al* (2019). We present new 21st century sea-level projections for South Asia tide gauge locations, developed using the outputs of CMIP5 models and the methods applied in UK Climate Projections 2018 (UKCP18) (Palmer *et al* 2018, Palmer *et al* 2020). The aims of this paper are to: (1) quantify the extent of relative local mean sea-level (hereafter LMSL) at tide gauge locations along the Indian Ocean coastline and compare to global mean sea-level (GMSL) changes; (2) identify the physical processes responsible for local departures in LMSL compared to GMSL changes; and (3) understand how contributions to LMSL changes and uncertainty ranges vary within the South Asia region.

In section 2 we present the datasets used in this study, including observed tide gauge and satellite altimeter data, climate model data and evidence from previous studies for other factors contributing to LMSL change. In section 3 we describe the methods used for constructing the new local sea-level projections. The new sea-level projections are provided in section 4, including a comparison between greenhouse gas concentration scenarios and discussion on the drivers behind spatial variations. The main findings are summarised and discussed in section 5, including limitations and potential future applications.

2. Data

2.1. Tide gauge data

Sea-level projections are generated for tide gauge locations across the South Asia region (figure 1). The locations were selected to span the spatial variations in future sea-level change over the region. Data was sourced from the Permanent Service for Mean Sea Level[3] (Holgate *et al* 2013) for locations with records of at least 60% completeness for the years 1990–2000 corresponding to the middle decade of the baseline period used by the projections, 1986–2005. Note that whilst Karachi did not satisfy this criterion, it has been included to highlight spatial gradients of sea-level change in the region. The latitude, longitude and data completeness over the baseline period are summarized in table S1 (supplementary materials). The tide gauge records were not corrected for vertical land movement, since the local sea-level projections used in this study include estimates for local glacial isostatic adjustment (GIA) and we want to retain GIA signal in the tide gauge records.

2.2. Satellite altimeter data

The satellite altimeter data used in this study is from v2.0 of the European Space Agency (ESA) Climate Change Initiative for Observations of sea level (CCI) described by (Legeais *et al* 2018). The ESA altimetry dataset is based on gridded observations from nine altimeter missions over the period 1993–2015, that provided monthly mean values for GMSL and two-dimensional fields on a 0.25° by 0.25° latitude-longitude grid. Gridded observations have been homegenised and reprocessed. Monthly mean gridded sea-level anomalies were converted to annual-mean anomalies to allow for comparisons with the local sea-level projections in this study and to supplement the tide gauge data described in section 2.1. The annual mean time-series are extracted from the closest grid box to the tide gauge locations (figure 1).

2.3. Climate model data

21 Global Climate Models (GCMs) are used in this study, taken from the climate model simulations carried out as part of CMIP5 (Taylor *et al* 2012). The sea-level projections in this study are based on the same CMIP5 model ensemble used for GMSL projections presented in the IPCC fifth assessment report (AR5) and the LMSL projections described by Palmer *et al* (2020). The list of the CMIP5 models used is summarized in table S2

[3] https://www.psmsl.org/data/.

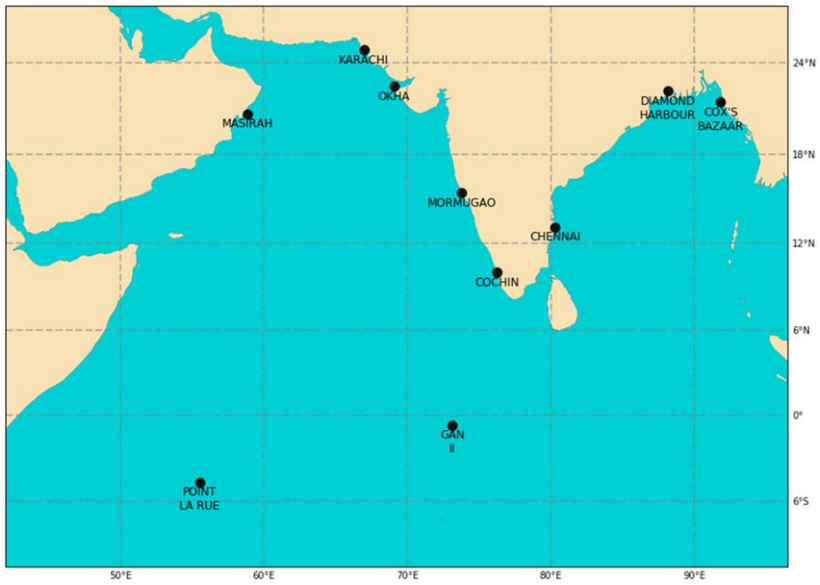

Figure 1. Locations of tide gauge stations for the tide gauge data, satellite altimeter observations and local sea-level projections used in this study.

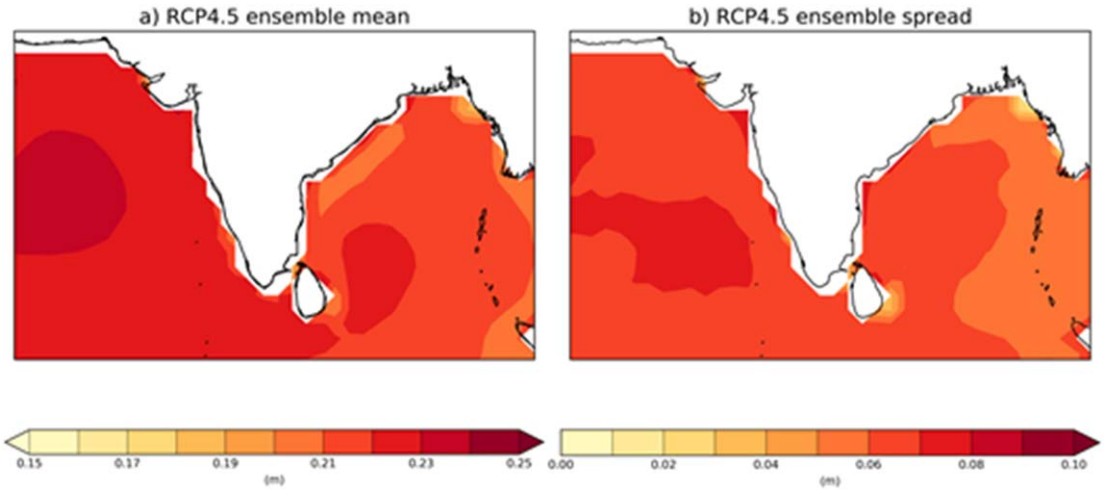

Figure 2. Projections of Indian Ocean sterodynamic sea-level change for 2081–2100 relative to 1986–2005 from an ensemble of 21 CMIP5 models: (a) ensemble mean; (b) ensemble spread at the 90% confidence interval based on the ensemble standard deviation. The spatial patterns come from the forced response of ocean dynamic sea-level across the CMIP5 model ensemble. Adapted from IPCC AR5 (Church *et al* 2013, figure 13.16).

(supplementary materials). Projections use simulations of global mean surface temperature (*tas*), global mean thermosteric sea-level rise (*zostoga*) and ocean dynamic sea level or sea surface height above geoid (*zos*) for the Representative Concentration Pathways (RCPs; Meinshausen *et al* 2011) RCP2.6, RCP4.5 and RCP8.5. The timeseries for ocean dynamic sea level and global mean thermosteric sea-level rise are drift-corrected with a quadratic fit to the corresponding pre-industrial control simulation for each model. The drift-correction is intended to remove any artificial signals arising from the ongoing spin-up of the deep ocean and/or limitations associated with representation of energy conservation within the model domain. The spatial pattern for sterodynamic sea-level change (zostoga + zos) over the South Asia region is shown for RCP4.5 (figure 2). More detailed descriptions of the projections and underlying datasets are provided in Palmer *et al* (2020).

2.4. Gravitation, rotation and deformation effects

Changes to the distribution of solid and liquid water mass on the Earth's land surface give rise to geographically varying patterns of sea-level change, due to the effect of mass redistribution on the Earth's gravitation, axial rotation and deformation of solid earth surface from mass loading (Tamisiea and Mitrovica 2011). Using the

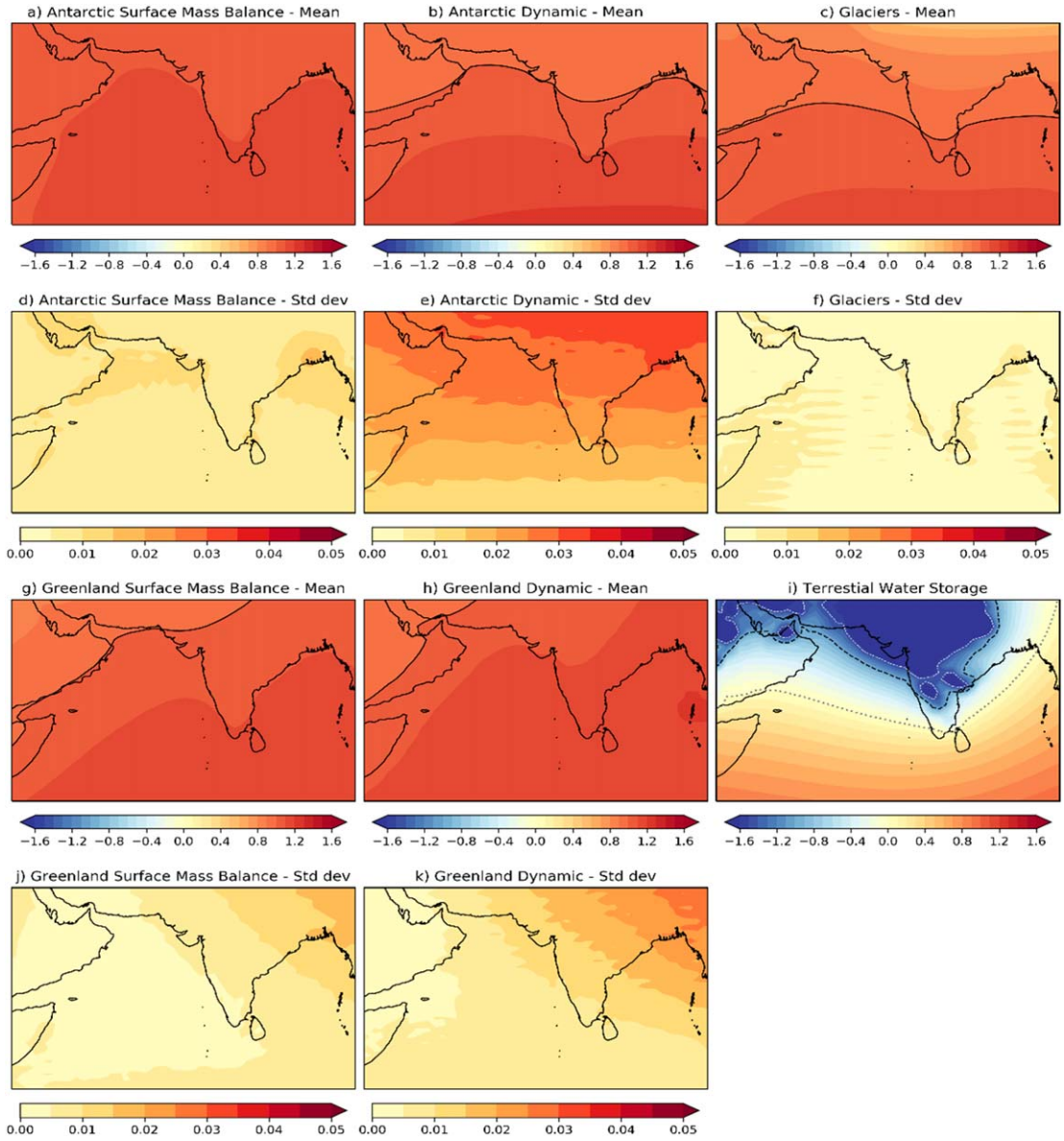

Figure 3. Estimates for local sea level changes arising from the effect of mass changes on Earth gravitation, rotation and deformation of the solid earth surface from mass redistribution. Panels (a)–(c), (g) and (h) show the mean of estimates from three GRD model solutions and the corresponding standard deviations are shown in (d)–(f), (j) and (k). The GRD estimate for land water storage is based on a single GRD model solution and therefore no standard deviation is shown. The GRD estimates represent scaling factors and are expressed as the LMSL change per unit rise in GMSL. The unit and zero contours are indicated by the solid and dotted lines respectively. In panel (i) the −1.0 and −1.5 contours are indicated by dashed lines black and grey lines respectively. Reproduced from Palmer *et al* 2020. CC BY 4.0.

nomenclature of Gregory *et al* (2019) we collectively refer to these as GRD (Gravity, Rotation, Deformation) effects. The GRD estimates are represented as scaling factors indicating the GRD contribution to LMSL change per unit of barystatic GMSL rise for each of the following (a) Antarctica surface mass balance, (ii) Antarctica ice dynamics, (iii) Greenland surface mass balance, (iv) Greenland ice dynamics, (v) glacier ice mass, and (vi) terrestrial water mass storage (figure 3).

Following Palmer *et al* (2020) we use three different estimates for GRD effects arising from ice mass changes at ice sheets and glaciers, produced by Spada and Stocchi (2007), Klemann and Groh (2013) and Slangen *et al* (2014). It should be noted that the locations of mass change are common across the three GRD estimates, therefore the results account for some of the uncertainty arising from the modelling of GRD effects but do not account for uncertainty in the locations of mass change.

A single estimate is used for GRD from changes in terrestrial liquid water mass storage (TWS), following Slangen *et al* (2014) and based on projections of GMSL rise equivalent from Wada *et al* (2012) and revised projections from Wada *et al* (2016). The locations of terrestrial water mass change are assumed to be the same for both the original and revised estimate, so that the spatial patterns are unchanged and the contributions differ in

magnitude only. The projections for future GMSL equivalent from (Wada *et al* 2012, 2016) represent the net contribution of TWS reductions from groundwater extraction and increases from impoundment of water in reservoirs, with the former process dominating over the 21st century for the projections used in this study. There is likely to be a large amount of uncertainty in 21st century TWS changes for locations in South Asia due to the construction of new reservoirs and population dependent groundwater use.

The region considered in this study is expected to feature areas of terrestrial water mass loss from groundwater extraction (figure 3(i)) but also new areas of terrestrial mass gain due to new reservoirs (Zarfl *et al* 2015, Hawley *et al* 2020). In the TWS GMSL projections from Wada *et al* (2012) it was assumed that all extracted groundwater would be transferred to the oceans, whereas according to Wada *et al* (2016) this assumption may overestimate the mass input to the oceans from groundwater extraction by up to 20%. We construct a second TWS GMSL time series by reducing positive TWS GMSL for years with positive increments in the Wada *et al* (2012) time series by 20%.

The spatial patterns for GRD effects over the study region arising from ice mass changes over Antarctica, glaciers and Greenland (figures 3(a)–(c), (g)–(h)) are characterized by weak spatial gradients and values that are close to unity. This indicates that contributions to LMSL change from GRD effects and contributions to GMSL from the mass changes are of the same sign and similar in magnitude. For the GRD spatial pattern from worldwide glacier ice mass loss (figure 3(c)) there is a weak meridional gradient, indicating an attenuation of the glacier component of GMSL change for the north of the study region, where reductions in Himalayan glacier ice results in weaker gravitational attraction between the landmass and the surrounding waters.

In contrast, the spatial pattern for GRD effects arising from TWS mass (figure 3(i), land water) changes features strong spatial gradients and changes in sign. The GMSL contribution from TWS is not only greatly attenuated by gradients in both the Arabian Sea and Bay of Bengal but also changes in sign, such that the contribution to LMSL changes is negative or zero along long stretches of coastline in this region. Since the mass change contributions to GMSL from the ice sheets and glaciers are much larger than from TWS, the GRD effects from TWS are not a significant driver of LMSL change but rather a driver of spatial variations in sea-level change.

2.5. Glacial isostatic adjustment (GIA)

Sea-level projections include estimates for contributions of Glacial Isostatic Adjustment (GIA) to LMSL change. GIA refers to the adjustment of the Earth's lithosphere and underlying viscous mantle towards hydrostatic equilibrium in response to the transfer of ice mass to oceans since the last glaciation (Tamisiea and Mitrovica 2011). The ongoing redistribution of mass is associated with GRD effects that determine the spatial patterns of sea-level change from GIA (e.g Shennan *et al* 2012). Since the adjustment process takes place over thousands of years (i.e. the response since the last glaciation), the rate of adjustment is treated as approximately constant for the multi-decadal and centennial sea-level projections in this study.

Following Palmer *et al* 2020, three global GIA estimates were used for the sea-level projections presented in this report. The estimates were based on the ICE-5G model (Peltier 2004), ICE-6G model (Argus *et al* 2014, Peltier *et al* 2015) and an independent estimate from the Australian National University based on an update of Nakada and Lambeck (1988). For the South Asia region, the ICE-5G and ICE-6G estimates show small differences in the position of the zero-line contour (figure S2 supplementary materials (available online at stacks.iop.org/ERC/3/115003/mmedia)), which is slightly further away from the Indian sub-continent land mass in the ICE-6G. In the Nakada and Lambeck (1988) GIA estimate, the contributions to sea-level change are less than 1 mm/year for much of the study region. The mean and standard deviation from the three GIA estimates (figure 4) indicate small contributions to local sea-level change from GIA and no significant contribution to overall uncertainty in sea-level from the choice of GIA model.

3. Methods

3.1. Global sea-level projections

The projections used in this study are based on methods developed for the United Kingdom Climate Projections 2018 (UKCP18, Lowe *et al* 2018) project, which presented time mean sea-level projections for UK tide gauge locations as part of UKCP18-Marine (Palmer *et al* 2018). We follow the methods of Palmer *et al* (2020) that extended the methods from UKCP18 to tide gauge locations around the world. In this section we provide a brief overview of the methodology used for sea-level projections at tide gauge locations in this study; see Palmer *et al* (2018) for further details.

The sea-level projections used in this study build on the Monte Carlo process-based GMSL projections presented in IPCC AR5 (Church *et al* 2013), based on climate simulations from the Coupled Model Intercomparison Project Phase 5 (CMIP5; Taylor *et al* 2012). The GMSL projections are taken directly from Palmer *et al* (2020), and include estimates for contributions to GMSL from: (i) global-mean thermosteric

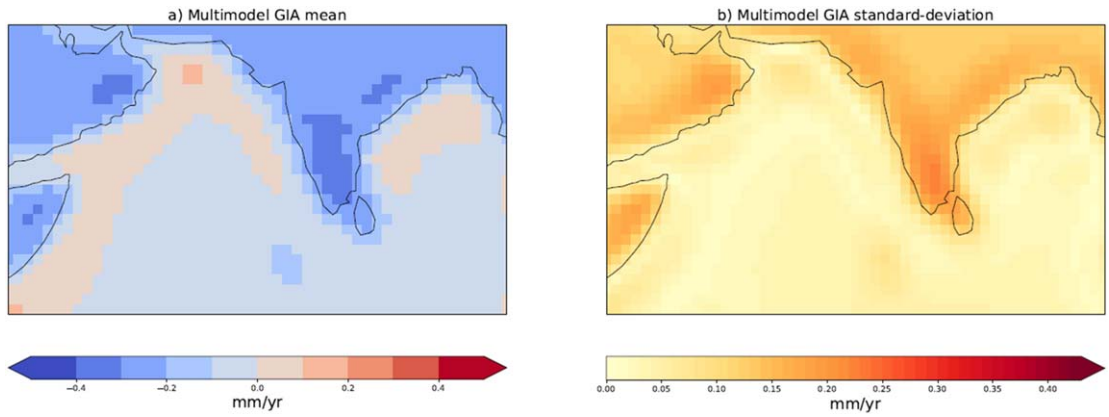

Figure 4. (a) Mean from ICE-5G, ICE-6G and Nakada and Lambeck (1988) model estimates of the effect of glacial isostatic adjustment (GIA) on sea-level change for the study region, and (b) standard deviation of the three GIA estimates.

sea-level change and six barystatic contributions to GMSL; (ii) Antarctica surface mass balance; (iii) Antarctica ice sheet dynamics; (iv) Greenland surface mass balance; (v) Greenland ice sheet dynamics; (vi) worldwide glaciers; and (vii) terrestrial water storage. The main innovation for the GMSL projections compared to IPCC AR5 is the inclusion of an updated, scenario dependent estimate for the Antarctic ice sheet dynamics contribution based on Levermann *et al* (2014). In this study we include a revised estimate for the GMSL contribution from terrestrial water storage mass changes based on Wada *et al* (2016).

3.2. Local sea-level projections

Following Palmer *et al* (2020), we account for contributions to LMSL change due to effects from ocean circulation (ocean dynamics) and ocean density (steric) by establishing regression relationships between global average thermal expansion (thermosteric) sea-level change and ocean dynamic sea level at the selected tide gauge locations for each of the 21 CMIP5 models. We adopt the terminology of Gregory *et al* (2019) and refer to the combined effect of local ocean dynamics and steric changes as sterodynamic sea-level change. The local projections are directly traceable to the same Monte Carlo procedure used for the GMSL projections in IPCC AR5. The four stages for obtaining the LMSL projections from the GMSL Monte Carlo are as follows:

1. Each instance of the 450,000-member Monte Carlo ensemble provides a set containing seven timeseries, with one time series for each of the seven components of GMSL. An instance is randomly drawn from the Monte Carlo ensemble, which provides a time series for each of the seven barystatic components of GMSL change.
2. Next, one of the available GRD models is randomly selected and the GRD spatial patterns are applied to time series for barystatic components of GMSL, providing time series for GRD contributions to LMSL at the tide gauge locations. Except for the land water storage component, the GRD patterns all use the same (randomly selected) GRD model. For the terrestrial water storage mass component, the contribution to LMSL is based on the single GRD solution of Slangen *et al* (2014). The GRD estimates each provide a time series for six components of LMSL change.
3. For each tide gauge location, we determine regression coefficients for the changes in sterodynamic sea level per increment of thermosteric GMSL rise in each of the 21 CMIP5 models. The remaining time series for thermosteric sea level change from the Monte Carlo instance is combined with a regression coefficient randomly selected from the 21 CMIP5 models. This results in a time series for the estimated sterodynamic sea-level change at each of the tide gauge locations.
4. The seven timeseries, corresponding to the six barystatic components and one sterodynamic component are combined with an estimate for the contribution due to GIA (section 2.5). The GIA estimate is provided by a random selection from one of the three GIA models. For each tide gauge location, the procedure is repeated 100,000 times to generate a distribution for projected LMSL changes, with each of the three RCP scenarios. As with IPCC AR5 GMSL projections, the spread is based on the 5th and 95th percentiles of the resulting distributions for the different components and for the combined LMSL change.

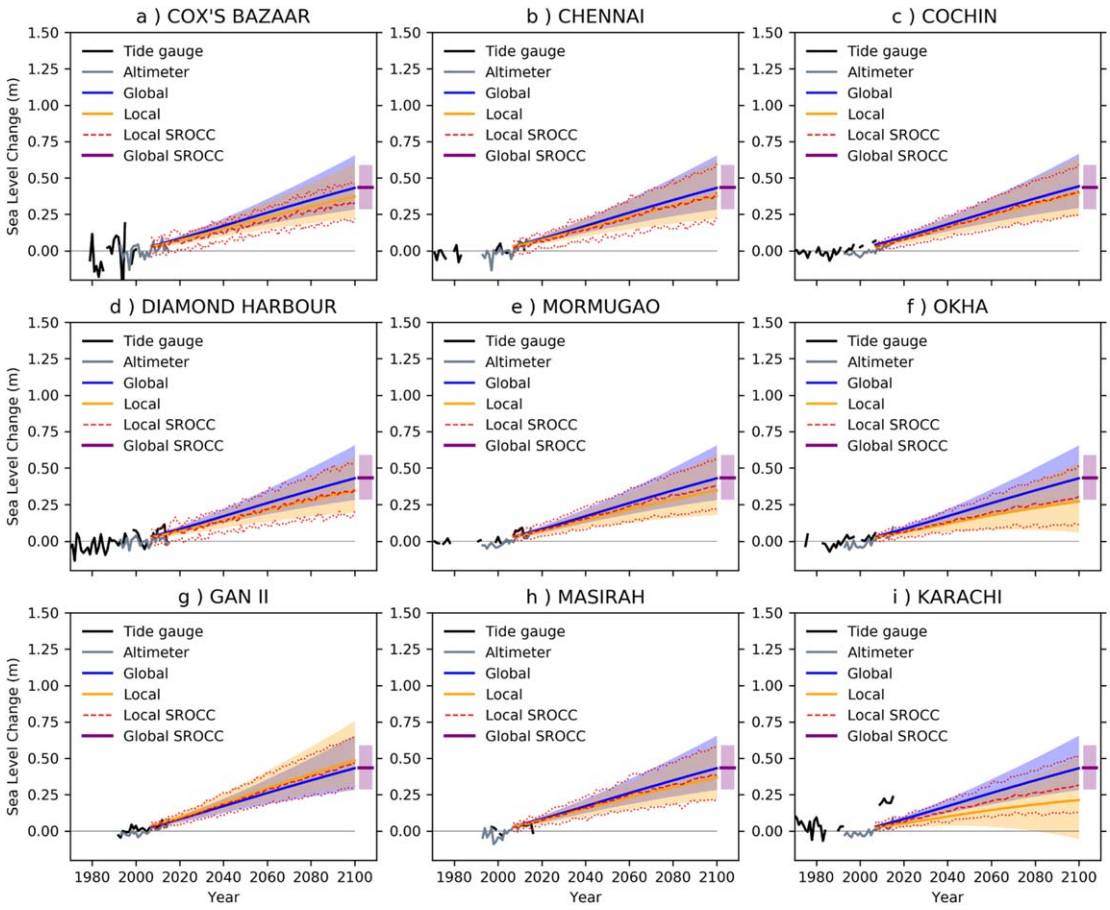

Figure 5. Local sea-level projections (yellow) and global sea-level projections (blue) for RCP2.6. Shaded regions indicate the 5th to 95th percentile range from a 100,000 member Monte Carlo simulation. The dotted red lines and purple bar indicate the 5th and 95th percentile of local and global projections from the IPCC SROCC (Oppenheimer *et al* 2019). Local annual mean sea-level from tide gauge records are shown in black. Local annual-mean satellite altimeter data are indicated by the solid grey line. All time series are shown relative to baseline period 1986–2005 average.

4. Results

4.1. Projected changes in local time mean sea-level

In this section we discuss the projected LMSL changes at selected tide gauge locations (figure 1). We focus our discussion on projections for RCP2.6 (figure 5) and RCP8.5 (figure 6) to illustrate the commitment to sea-level rise for scenarios with contrasting trajectories for greenhouse gas emissions over the 21st century. The corresponding figures/tables for RCP4.5 are included in the supplementary material. The LMSL changes for RCP4.5 lie within the range spanned by RCP2.6 and RCP8.5.

To demonstrate recent sea-level trends and variability, we include time series of relative and geocentric annual mean sea-level, from tide gauge and satellite altimetry data respectively. In general the time series are expected to differ due to vertical land movement (VLM) at the tide gauge location. The tide gauge data will contain additional contributions from VLM processes associated with local subsidence and/or tectonic activity, whereas the altimeter time series reflects changes relative to fixed reference geoid. In general, over the period 2007–2015, we see agreement in the sea-level change trends from the satellite altimetry and projection time series. The projection time series do include VLM contributions from GRD (through viscoelastic deformation) effects associated with GIA (section 2.5) but for the tide gauge locations in this study the GIA effects are small.

The only locations with sufficient tide gauge data coverage for 2007–2020 (initial part of the projection period) are Diamond Harbour (West Bengal, India), Gan II (Addu Atoll, Maldives) and Okha (Gujarat, India). For Diamond Harbour (figures 5(d) and 6(d)), we see differences in the tide gauge records relative to the altimetry and projection time series, which could be attributed to the tide gauge being situated on an inland waterway (Houghly River), where there are additional contributions associated with variability in fresh-water run-off. For Okha (figures 5(f) and 6(f)) and Gan II (figures 5(g) and 6(g)) we see better agreement in the tide gauge and altimeter time series, and trends for the initial period of the projection time series. For the Karachi tide

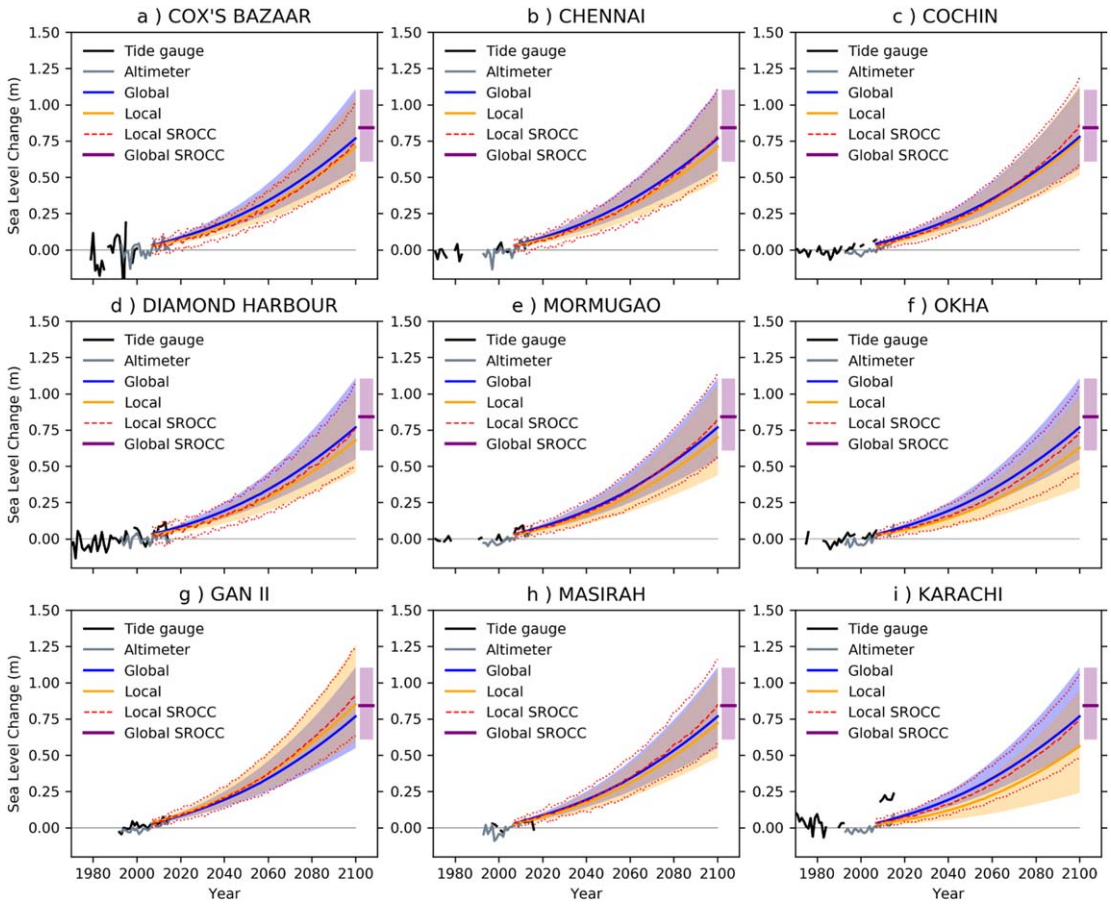

Figure 6. Local sea-level projections (yellow) and global sea-level projections (blue) for RCP8.5. Shaded regions indicate the 5th to 95th percentile range from a 100,000 member Monte Carlo simulation. The dotted red lines and purple bar indicate the 5th and 95th percentile of local and global projections from the IPCC SROCC (Oppenheimer *et al* 2019). Local annual mean sea-level from tide gauge records are shown in black. Local annual-mean satellite altimeter data are indicated by the solid grey line. All time series are shown relative to baseline period 1986–2005 average.

gauge time series there is no data for the period 1993–2006 and data from 2007 onwards is from an instrument at a different site.

In order to investigate the effects of different projection methods on future LMSL change, we compared the local projections generated for this study with projections based on data provided in IPCC Special Report on Oceans and Cryosphere in a Changing Climate (SROCC; Oppenheimer *et al* 2019). In general there is agreement between the two projection methods for most of the tide gauge locations, except for tide gauge locations in the northern Arabian Sea (e.g. Okha and Karachi) where the SROCC projections are higher. The mismatch between the projection in this study and those from SROCC over the north Arabian Sea are thought to arise from differences in GRD fingerprints used to estimate the terrestrial water storage contribution to LMSL change (A. Slangen, personal communication). The largest differences are seen at Karachi and decrease for locations to the east (e.g. Masirah, figures 5(h), 6(h)) and south (e.g. Okha figures 5(f) and 6(f)) along spatial gradients for the terrestrial water storage component of LMSL change from GRD effects (figure 3(i)).

Compared to projected GMSL changes, the projected LMSL changes span a wider range reflecting the greater uncertainty at the local scale. For most tide gauge locations the magnitude of projected LMSL change is smaller than projected GMSL change under RCP2.6. The exception is Gan II (figure 5(g)), where the departure of LMSL change from GMSL change is positive but small. For all locations, excluding Gan II, the local departures from GMSL change are smaller under RCP8.5. At Gan II the local excess relative to GMSL change is larger under RCP8.5 (figure 6(g)) and this can also be seen in the SROCC projections. This effect arises from the increased contribution from ice mass changes to GMSL, which result in spatially uniform local changes of similar magnitude from GRD effects (figures 3(a), (b), (g) and (h)).

4.2. Drivers of LMSL change and spatial variations

The LMSL projections for the tide gauge locations in this study highlight notable variations in LMSL change relative to GMSL changes as well as spatial variations of LMSL change across the South Asia region. The

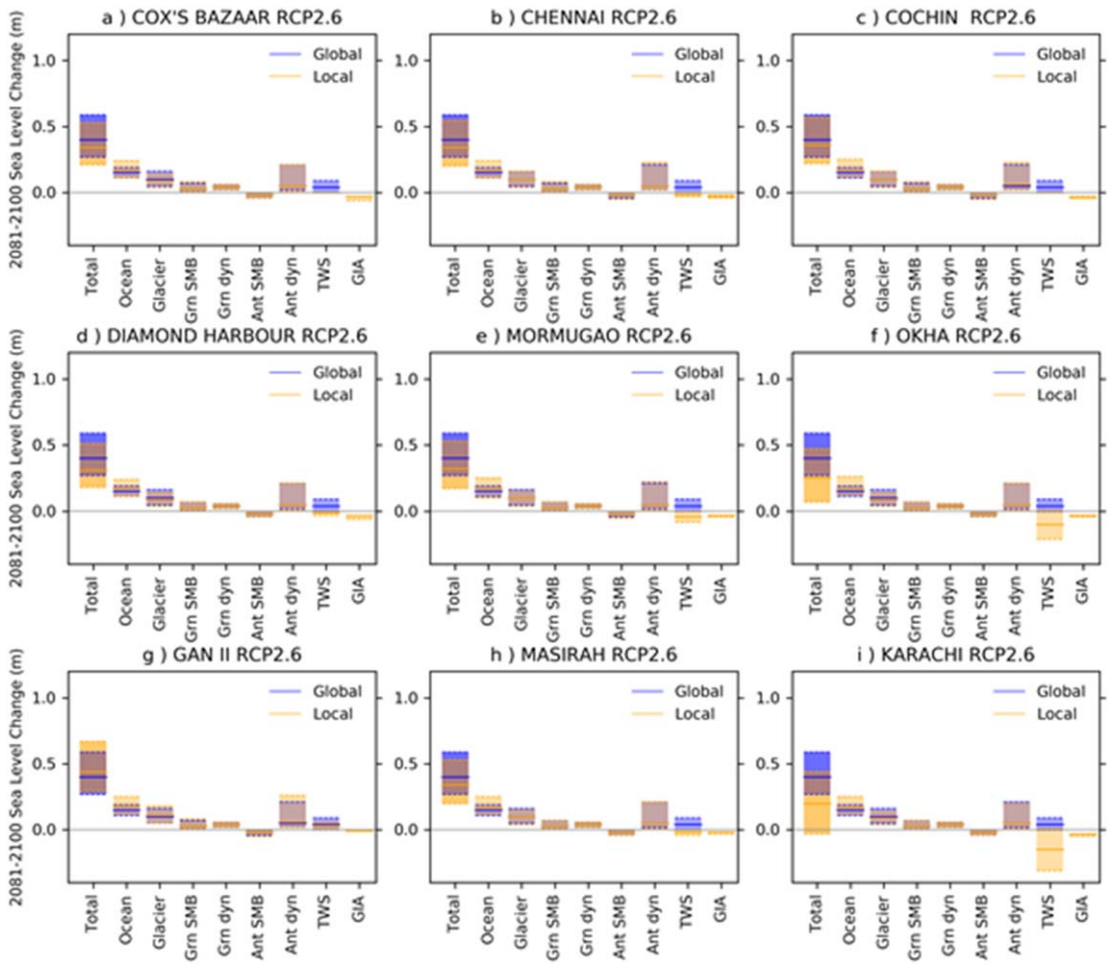

Figure 7. Components of projected local mean sea-level change (yellow) and global mean sea-level change (blue) for 2081–2100 under RCP2.6. The horizontal lines and shaded regions indicate the 50th percentile and 5th to 95th percentile range respectively from the 100,000 member Monte Carlo ensemble. All projections are expressed relative to the baseline period 1986–2005 average. The ocean component refers to sterodynamic sea-level change for the local projections and thermosteric (ocean thermal expansion) for the global projections. Glacial isostatic adjustment (GIA) does not make a net contribution to global mean seal level changes and the GIA component refers only to local mean sea level changes.

magnitude of the regional departure from GMSL change and the within region spatial gradients of LMSL change, both depend on the climate scenario and are smaller in magnitude for RCP8.5 compared to RCP2.6. The tendency for South Asia LMSL changes to become more spatially homogeneous and more similar to the global average, arises from GRD effects associated with the increased contributions to GMSL rise from ice mass losses under RCP8.5. The GRD fingerprints from Antarctica and Greenland ice mass changes feature generally spatially homogeneous, greater than unity, values over South Asia. The region lies in the far-field relative to these areas of mass change and the contributions to LMSL change from GRD effects are larger in magnitude than the corresponding contributions to GMSL change by 5%–15%. The reduced spatial heterogeneity in LMSL change under the stronger forcing scenario also arises from increases in the sterodynamic contribution to LMSL change, since sterodynamic changes are broadly consistent across the region and about 10% larger than the corresponding increase in the thermosteric contribution to GMSL change.

The departure of LMSL changes from GMSL change over South Asia is driven by scenario independent GRD effects from TWS changes. Groundwater depletion over the sub-continent corresponds to a broad area of TWS mass loss. The GRD effects from TWS mass changes (figure 3(i)) result in negative near-field and positive far-field contributions to LMSL change. Contributions from other physical processes to the 21st century are generally similar under RCP2.6 (figure 7) and RCP8.5 (figure 8). For TWS the LMSL contributions are less than the GMSL contribution, with negative (Karachi, figure 7(i)) or zero (Cox's Bazaar, figure 7(i)) contribution at the tide gauge locations.

The projections reveal spatial gradients in LMSL changes across the South Asia region. Projected LMSL changes are larger for equatorward locations, where there are larger contributions from GRD effects from terrestrial ice (Antarctica ice dynamics; figure 3(b), glaciers figure 3(c)) and water mass losses (figure 3(i)). The gradients of LMSL changes arising from GRD effects associated with ice mass losses are weak compared to GRD

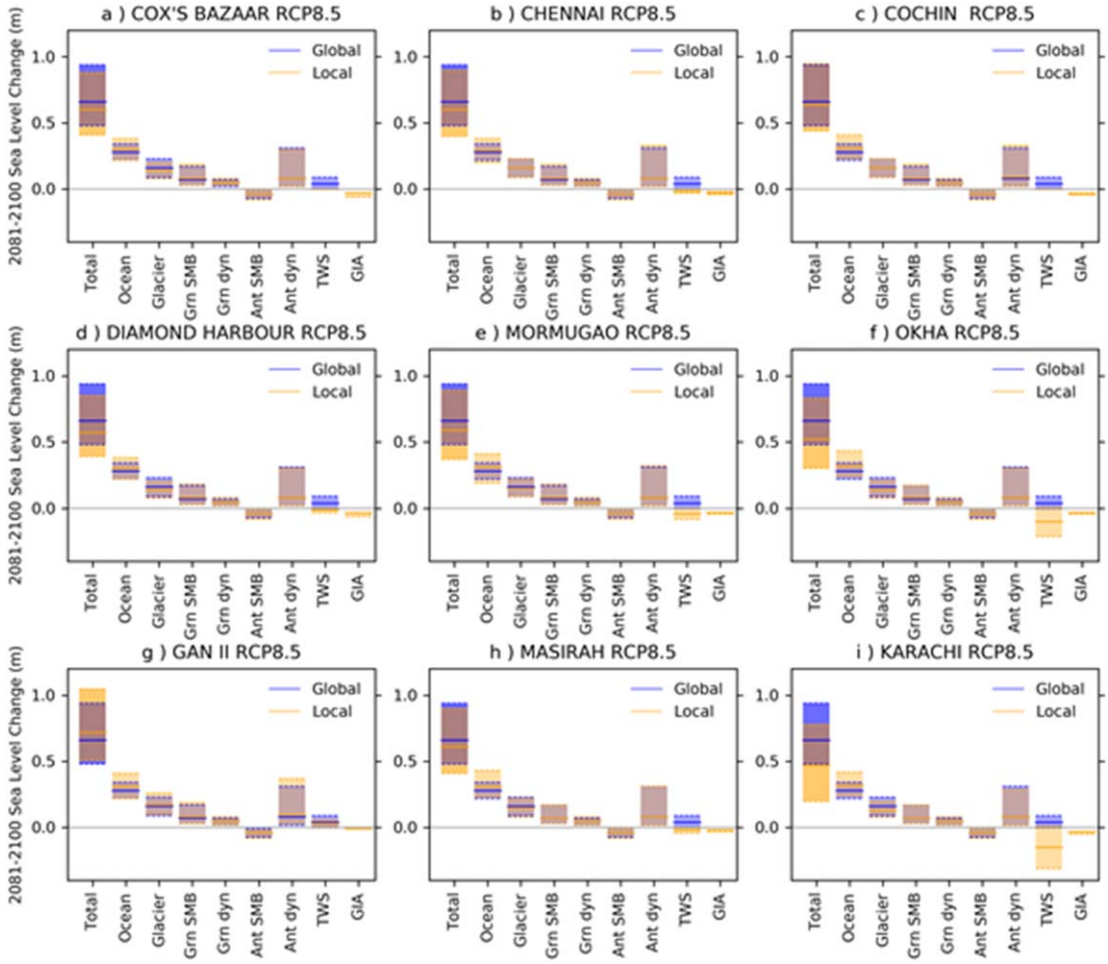

Figure 8. Components of projected local mean sea-level change (yellow) and global mean sea-level change (blue) for 2081–2100 under RCP8.5. The horizontal lines and shaded regions indicate the 50th percentile and 5th to 95th percentile range respectively from the 100,000 member Monte Carlo ensemble. All projections are expressed relative to the baseline period 1986–2005 average. The ocean component refers to sterodynamic sea-level change for the local projections and thermosteric (ocean thermal expansion) for the global projections. Glacial isostatic adjustment (GIA) does not make a net contribution to global mean seal level changes and the GIA component refers only to local mean sea-level changes.

effects from terrestrial water mass loss but the contributions are larger in magnitude. There are also zonal gradients of LMSL change, due to the GRD effects of TWS mass changes. LMSL changes decrease westward along the northern coast of the Arabian sea and eastward for the northern coast of the Bay of Bengal. The TWS contribution determines both the within region variations of LMSL changes and the regional departure of LMSL changes from GMSL change.

We expect there is significant unquantified structural uncertainty for the TWS change contribution to GMSL rise and for the locations of TWS mass loss used to determine the TWS GRD effects. The TWS contribution for GMSL from AR5 is likely an overestimate, since the time series assumed all TWS mass losses are gained by the oceans. Subsequent estimates from Wada *et al* (2016) suggest that the fraction of TWS water mass transferred to the oceans is 80%. To determine the impact of the effect on South Asia LMSL changes, we applied a correction to each year in the TWS time series with positive values, reducing the magnitude by 20%. GRD effects from the implied reduction in TWS mass losses result in a decrease in overall LMSL change at tide gauge locations in the equatorial Indian ocean (Gann II; Maldives, Point La Rue; Seychelles). However, for most tide gauge locations LMSL changes increase due to the reduced near-field negative contribution from TWS GRD effects (figure 9).

In time series for contributions from TWS mass changes to 21st century GMSL rise, mass losses from groundwater depletion are assumed to dominate over mass gains from reservoir impoundment. In the Wada *et al* (2012) estimate this occurs for the first decade of the 21st century. However impoundment could remain dominant until the mid 21st century, due to additional impoundment artificial reservoirs currently under construction (Hawley *et al* 2020). As with groundwater depletion the impact of TWS mass changes from impoundment on LMSL changes will depend on the locations of mass change. During the mid 20th century, the South Asia region saw a boom in dam construction and regional increases in TWS mass storage. Over 100 new

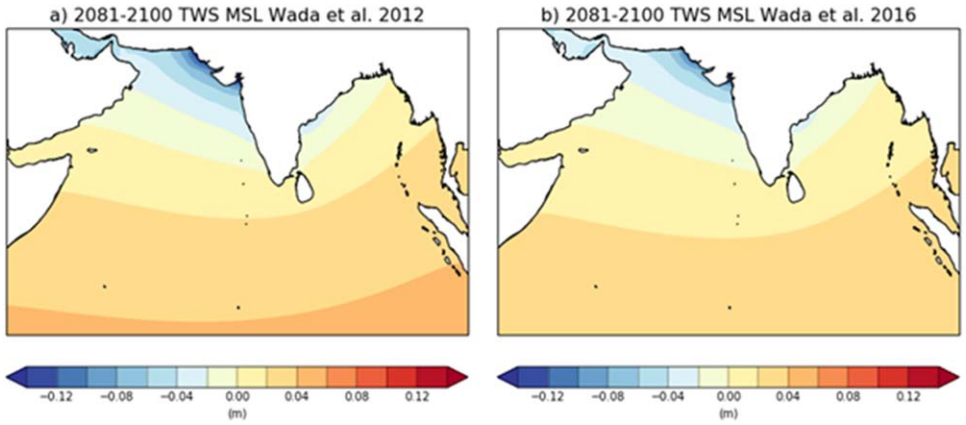

Figure 9. Local sea-level changes from gravitation, rotation and deformation (GRD) effects of terrestrial water storage (TWS) mass changes for the period 2081–2100 relative to the baseline period 1986–2005 average based on central estimates of time series for TWS GMSL contribution from (a) Wada *et al* 2012 and (b) Wada *et al* 2016.

dams are also planned or under construction over the 21st century but groundwater extraction is expected to continue with rising water demand from the combination of increased population density and reductions in groundwater recharge under a warmer climate (Zarfl *et al* 2015). In our analysis we used the scenario independent estimate for the TWS contribution to GMSL change but scenarios make different assumptions about population, which together with differences in climate factors that influence groundwater recharge would imply scenario dependent TWS changes.

The sea-level projections account for contributions to relative sea-level changes from GIA-related vertical land movement (VLM) but do not account for local scale processes such as sediment dynamics, tectonic activity and subsidence. Estimates of recent sea-level trends from tide gauge records in the Ganges-Brahmaputra-Meghna basin, indicate that contributions from subsidence to rate of relative sea-level change could be −18.0 to 0.0 mm year^{-1}, so are larger or comparable to the expected rates from climate change contributions (Higgins *et al* 2014, Becker *et al* 2020, Nicholls et al 2021). In South Asia, a tectonically active region, earthquakes can induce VLM through discrete uplift events. For some regions, such as the Balochistan provincial coastline in Pakistan, an average tectonic uplift rate over the past 10,000 years of 1–2 mm year^{-1} (Page *et al* 1979) has been assumed in studies to 'balance' the effects of GMSL rise (Weeks and Harrison 2020). Since tectonic activity is discontinuous, the actual rate varies both spatially and temporally, and a single event could cause vertical displacement on the order of metres. Contributions of non-GIA vertical land movement processes are likely to be more important than GRD effects from TWS in determining spatial variations in current rates of relative sea-level change.

4.3. Robustness of LMSL projections

The sea-level projections are premised on an ensemble of climate models from CMIP5, that formed the basis of the GMSL projections presented in IPCC AR5. While there was substantial improvement in representation of ocean dynamic sea level in CMIP5 model compared to the processor CMIP3 models (Landerer *et al* 2014, Meehl *et al* 2007), the differences between models from CMIP5 and successor CMIP6 (Eyring *et al* 2016) are less significant and mainly found in the southern hemisphere at high latitudes (Lyu *et al* 2020). Projections of global thermosteric sea-level change from CMIP5 and CMIP6 models are not substantially different over the 21st century (Jevrejeva *et al* 2020). GMSL projections generated with CMIP6 data following the methods AR5 from the CMIP5 based projections over the 5th–95th percentile range of the distribution, by an additional of 3–7 cm and 2–3 cm for median changes, depending on the scenario (Hermans *et al* 2021). Another finding from Hermans *et al* (2021) is that the 5th–95th percentile range for CMIP6 thermosteric GMSL projections have widened compared to CMIP5 but mostly towards lower values, decreasing by 2cm and 4 cm at the 5th percentile for SSP1-RCP2.6 and SSP5-RCP8.5 respectively and increasing by 1cm at the 95th percentile. We expect similar impacts for the LSML projections in this study, since (1) the methods directly traceable to the AR5 GMSL projections, (2) the scenario dependent barystatic contributions to sea-level from GRD in this region are spatially uniform, and (3) spatial patterns of sterodynamic change in the region are consistent between CMIP5 and CMIP6 models. While the magnitudes of sea-level change by the end of the 21st century are similar for the different generation climate models, the rates of change at 2100 substantially higher in the CMIP6 projections, increasing by 0.4 mm yr^{-1} for SSP1-RCP2.6 and 1.4 mm yr^{-1} for SSP5-RCP8.5 (Hermans *et al* 2021). For post

2100 LMSL projections for this region, as included in Harrison *et al* (2020), we cannot rule out substantial differences between CMIP5 and CMIP6 based projections.

5. Conclusions

In this study, new sea-level projections over the 21st century are presented for tide gauge locations in South Asia. The projections focus on locations along the coastlines of the Arabian Sea, Bay of Bengal and islands in the equatorial Indian Ocean. Local sea-level projections were calculated using the process-based approach of the GMSL projection in IPCC AR5 and SROCC, with an ensemble constructed using the same 21 CMIP5 GCMs. The local sea-level projections were used to estimate spatial variations in future sea-level change over the South Asia region, for future climate scenarios with low (RCP2.6) and high (RCP8.5) greenhouse gas concentrations. Local sea-level projections were compared with global sea-level projections to estimate the extent to which local and regional sea-level changes could differ from GMSL changes, under contrasting future climate scenarios.

In our study we show that the 5th–95th percentile range for GMSL changes for the end of the 21st century (2081–2100) are 0.27 to 0.59 m under RCP2.6 and 0.48 to 0.94 m under RCP8.5, with central estimates of 0.40 m and 0.66 m respectively. For coastal tide gauge locations in the north-east Arabian sea, such as Karachi, the 5th-95th percentile range for time mean sea-level changes at the end of 21st century are −0.03 to 0.44 m under RCP2.6 and 0.21 to 0.78 m under RCP8.5, with central estimates of 0.20 m and 0.47 m respectively. The central estimates for LMSL changes are approximately 50% and 30% lower than GMSL changes for RCP2.6 and RCP8.5 by the end of the 21st century. In the Arabian Sea the magnitude of differences between local and GMSL changes decreases westward. For Masirah in Oman the central estimates for sea-level changes at the end of the 21st century are around 40% and 20% lower than global changes under RCP2.6 and RCP8.5 respectively

For tide gauge locations on the northern coast of the Bay of Bengal, such as Diamond Harbour, the 5th-95th percentile ranges are 0.18 to 0.51 m and 0.39 to 0.85 under RCP2.6 and RCP8.5 respectively, with central estimates of 0.37 m and 0.57 m. The central estimates for LMSL changes at Diamond harbour are around 20% and 15% lower under RCP2.6 and RCP8.5 respectively. In the Bay of Bengal the magnitude of differences between local and GMSL changes decreases eastward. For Cox's Bazaar in Bangladesh the central estimates for LMSL changes at the end of the 21st are around 15% lower than global changes for RCP2.6 and 10% under RCP8.5. For tide gauge locations in the equatorial Indian Ocean, such as Gan II in the Maldives, the central estimates of LMSL changes for the end of the 21st century are around 10% greater than GMSL changes under both RCP2.6 and RCP8.5.

The spatial gradients of sea-level change over the South Asia region, and the departure of LMSL changes from GMSL changes, are largely determined by GRD effects arising from terrestrial water storage mass changes. The projected loss of terrestrial water mass stored on the subcontinent land mass from projected groundwater depletion, results in near-field decreases in sea-level rise and far-field increases in sea-level rise. The projected terrestrial water mass storage change are scenario independent and the relative importance of contributions to LMSL change through GRD effects diminishes under RCP8.5, due to the increased contributions from spatially uniform scenario dependent changes in sterodynamic sea-level and GRD effects arising from glacier or ice sheet mass changes.

The 21st century LMSL projections for South Asia tide gauge locations highlight the importance of future changes in terrestrial water storage in determining the departure of South Asia regional sea-level changes from future GMSL changes. The results are premised on a single estimate for GRD effects arising from changes in terrestrial water mass storage. Future changes in terrestrial water storage mass may be determined by mass losses from groundwater depletion and mass gains from reservoir impoundment. As with estimates for GRD effects arising from terrestrial ice mass loss, the locations of mass change are assumed to be fixed over the 21st century. Whilst this assumption is reasonable for locations of terrestrial ice mass change (ice sheets and worldwide glaciers), newly constructed dams and reservoirs could lead to distributions of terrestrial water mass changes that differ from the fixed location used by the single GRD estimate in this study.

The LMSL projections in this study are based on the 5th to 95th percentile range from the climate model distributions, corresponding to the 'likely range' in the calibrated language of the IPCC reports. We cannot rule out LMSL changes beyond the 5th to 95th percentile range of the projections from this study. Since the publication of IPCC AR5 several studies have highlighted the potential for substantial additional contributions to GMSL from Antarctic ice mass loss associated with ice sheet instability processes with GMSL rise in excess of 1m by 2100 for the most extreme scenarios, and much larger contributions in the centuries that follow (e.g. DeConto and Pollard 2016, Edwards *et al* 2019). The additional contribution to the LMSL projections will be modulated by the GRD effects arising from the Antarctica ice mass losses (see figure 3), which suggest similar magnitude increases in LMSL and GMSL from ice mass loss along the Bangladesh coast (GRD values 1.0–1.05) and for the Maldives an increase 10%–15% higher than the additional GMSL ice loss contribution. These

estimates are in line with calculations in Frederikse *et al* (2020), showing that for the IPCC AR5 LMSL projections show an Antarctic ice sheet contribution of 45 cm (60 cm) under RCP8.5 would contribute to total LMSL changes of 0.9m (1.1m) and 1.1m (1.3m) at Cox's Bazaar, Bangladesh and Gan II, Maldives respectively. Since IPCC AR5, several studies have highlighted the need for information on the potential high-end sea-level response (Le Cozannet *et al* 2017, Hinkel *et al* 2019, Stammer *et al* 2019) and narratives (such as the H^{++} scenario presented in Lowe *et al* 2009) as well as advancing methodology to introduce additional sources of uncertainty into the probabilistic distribution. Decision makers would benefit from incorporating these additional strands of evidence to develop comprehensive coastal risk, impact and adaptation assessments based on sea-level climate information.

Acknowledgments

This work was supported by the Asia Regional Resilience to a Changing Climate (ARRCC) programme, funded by the UK's Foreign, Commonwealth and Development Office (FCDO). The work also draws on advances made in the UK Climate Resilience programme supported by the UKRI Strategic Priorities Fund (SPF). SPF is co-delivered by the Met Office and NERC on behalf of UKRI partners AHRC, EPSRC, ESRC.

Data availability statement

The data that support the findings of this study are available upon reasonable request from the authors.

ORCID iDs

Benjamin J Harrison https://orcid.org/0000-0002-0007-6043
Joseph D Daron https://orcid.org/0000-0003-1917-0264
Matthew D Palmer https://orcid.org/0000-0001-7422-198X
Jennifer H Weeks https://orcid.org/0000-0002-9929-8147

References

Argus D F *et al* 2014 The Antarctica component of postglacial rebound model ICE-6G_C (VM5a) based on GPS positioning, exposure age dating of ice thicknesses, and relative sea level histories *Geophysical Journal International* **198** 537–63

Becker M *et al* 2020 Water level changes, subsidence, and sea level rise in the Ganges-Brahmaputra-Meghna delta *Proceedings of the National Academy of Sciences* **117** 1867–76

Brecht H *et al* 2012 Sea-level rise and storm surges: High stakes for a small number of developing countries *The Journal of Environment & Development* **21** 120–38

Church J A *et al* 2013 Sea Level Change. *Climate Change 2013: The Physical Science Basis. Contribution of Working Group I to the Fifth Assessment Report of the Intergovernmental Panel on Climate Change* (https://ipcc.ch/site/assets/uploads/2018/02/WG1AR5_Chapter13_FINAL.pdf)

DeConto R M and Pollard D 2016 Contribution of Antarctica to past and future sea-level rise *Nature* **531** 591–7

Edwards T L *et al* 2019 Revisiting Antarctic ice loss due to marine ice-cliff instability *Nature* **566** 58–64

Eyring V *et al* 2019 Overview of the Coupled Model Intercomparison Project Phase 6 (CMIP6) experimental design and organization *Geoscientific Model Development*. Copernicus GmbH, **9** 1937–58

Frederikse T *et al* 2020 Antarctic Ice Sheet and emission scenario controls on 21st-century extreme sea-level changes *Nature Communications* **11** 1–11

Gregory J M *et al* 2019 Concepts and terminology for sea level: Mean, variability and change, both local and global *Surveys in Geophysics* **40** 1251–89

Harrison B J *et al* 2020 *Sea level projections for South Asia Report on main findings* Met Office (https://metoffice.gov.uk/binaries/content/assets/metofficegovuk/pdf/business/international/report-on-regional-sea-level-projections-for-south-asia—arrcc-report—external-1.pdf)

Hawley W B *et al* 2020 A spatially variable time series of sea level change due to artificial water impoundment *Earth's Future* **8** e2020EF001497

Hermans T H J *et al* 2021 Projecting global mean sea-level change using CMIP6 models *Geophysical Research Letters* **48** e2020GL092064

Higgins S A *et al* 2014 InSAR measurements of compaction and subsidence in the Ganges-Brahmaputra Delta, Bangladesh *Journal Of Geophysical Research: Earth Surface* **119** 1768–81

Hijioka Y *et al* 2014 Asia. In: Climate Change 2014: Impacts, Adaptation, and Vulnerability *Part B: Regional Aspects. Contribution of Working Group II to the Fifth Assessment Report of the Intergovernmental Panel on Climate Change* ed V R Barros *et al* (Cambridge: Cambridge University Press) pp 1327–70

Hinkel J *et al* 2019 Meeting user needs for sea level rise information: a decision analysis perspective *Earth's Future* **7** 320–37

Holgate S J *et al* 2013 New data systems and products at the permanent service for mean sea level *Journal of Coastal Research* **29** 493–504

Jevrejeva S, Palanisamy H and Jackson L P 2020 Global mean thermosteric sea level projections by 2100 in CMIP6 climate models *Environmental Research Letters* **16** 014028

Jisan M A, Bao S and Pietrafesa L J 2018 Ensemble projection of the sea level rise impact on storm surge and inundation at the coast of Bangladesh *Natural Hazards and Earth System Sciences* **18** 351–64

Kay S *et al* 2015 Modelling the increased frequency of extreme sea levels in the Ganges–Brahmaputra–Meghna delta due to sea level rise and other effects of climate change *Environmental Science: Processes & Impacts* **17** 1311–22
Klemann V and Groh A 2013 Practical: Ice and loading *Lecture notes from the Summer School of DFG SPP1257 Global Water Cycle* (*Schriftenreihe Institut für Geodäsie und Geoinformation*) ed A Eicker and J Kusche **30** 227–36 (https://hdl.handle.net/20.500.11811/1424) Universität Bonn, Institut für Geodäsie und Geoinformation
Landerer FW, Gleckler PJ and Lee T 2014 Evaluation of CMIP5 dynamic sea surface height multi-model simulations against satellite observations. *Climate Dynamics* **43** 1271–83
Le Cozannet G *et al* 2017 Sea level change and coastal climate services: the way forward *Journal of Marine Science and Engineering.* **5** 49
Legeais J-F *et al* 2018 An improved and homogeneous altimeter sea level record from the ESA Climate Change Initiative *Earth System Science Data* **10** 281–301
Levermann A *et al* 2014 Projecting Antarctic ice discharge using response functions from SeaRISE ice-sheet models *Earth System Dynamics* **5** 271–93
Lowe J A *et al* 2009 *UK Climate Projections science report: Marine and coastal projections* Met Office Hadley Centre (http://ukclimateprojections.defra.gov.uk)
Lowe J A *et al* 2018 *UKCP18 Science Overview Report* Met Office Hadley Centre (www.metoffice.gov.ukwww.metoffice.gov.uk)
Lyu K, Zhang X and Church J A 2020 Regional dynamic sea level simulated in the CMIP5 and CMIP6 models: mean biases, future projections, and their linkages *Journal of Climate* **33** 6377–98
Meehl G A *et al* 2007 The WCRP CMIP3 multimodel dataset: A new era in climate change research *Bulletin of the American Meteorological Society* **88** 1383–94
Meinshausen M *et al* 2011 The RCP greenhouse gas concentrations and their extensions from 1765 to 2300 *Climate Change* **109** 213–41
Mitrovica J X *et al* 2001 Recent mass balance of polar ice sheets inferred from patterns of global sea-level change *Nature* **409** 1026–9
Nakada M and Lambeck K 1988 The melting history of the late Pleistocene Antarctic ice sheet *Nature* **333** 36–40
Nicholls R J *et al* 2021 Integrating new sea-level scenarios into coastal risk and adaptation assessments: An ongoing process *Wiley Interdisciplinary Reviews: Climate Change* **12** e706
Oppenheimer M *et al* 2019 Sea level rise and implications for low-lying islands, coasts and communities *IPCC Special Report on the Ocean and Cryosphere in a Changing Climate* 321–445
Page W D *et al* 1979 Evidence for the recurrence of large-magnitude earthquakes along the Makran coast of Iran and Pakistan *Tectonophysics* **52** 533–47
Palmer M *et al* 2018 *UKCP18 Marine Report* Met Office Hadley Centre (https://metoffice.gov.uk/research/approach/collaboration/ukcp/marine-projections)
Palmer M *et al* 2020 Exploring the drivers of global and local sea-level change over the 21st century and beyond *Earth's Future* **8** e2019EF001413
Peltier W R 2004 Global glacial isostasy and the surface of the ice-age earth: the ICE-5G (VM2) model and GRACE *Annual Review of Earth and Planetary Sciences* **32** 111–49
Peltier W R, Argus D F and Drummond R 2015 Space geodesy constrains ice age terminal deglaciation: the global ICE-6G_C (VM5a) model *Journal of Geophysical Research: Solid Earth* **120** 450–87
Rahman S *et al* 2019 Projected changes of inundation of cyclonic storms in the Ganges–Brahmaputra–Meghna delta of Bangladesh due to SLR by 2100 *Journal of Earth System Science* **128** 145
Shennan I, Milne G and Bradley S 2012 Late Holocene vertical land motion and relative sea-level changes: lessons from the British Isles *Journal of Quaternary Science* **27** 64–70
Slangen A B A *et al* 2014 Projecting twenty-first century regional sea-level changes *Climatic Change* **124** 317–32
Spada G and Stocchi P 2007 SELEN: a Fortran 90 program for solving the 'sea-level equation' *Computers and Geosciences.* **33** 538–62
Stammer D *et al* 2013 Causes for contemporary regional sea level changes *Annual Review of Marine Science* **5** 21–46
Stammer D *et al* 2019 Framework for high-end estimates of sea level rise for stakeholder applications *Earth's Future* **7** 923–38
Swapna P *et al* 2020 Sea-Level Rise *Assessment of Climate Change over the Indian Region.* (Singapore: Springer Singapore) 175–89
Tamisiea M and Mitrovica J 2011 The moving boundaries of sea level change: understanding the origins of geographic variability *Oceanography* **24** 24–39
Taylor K E, Stouffer R J and Meehl G A 2012 An overview of CMIP5 and the experiment design *Bulletin of the American Meteorological Society* **93** 485–98
Wada Y *et al* 2012 Past and future contribution of global groundwater depletion to sea-level rise *Geophysical Research Letters* **39** L09402
Wada Y *et al* 2016 Fate of water pumped from underground and contributions to sea-level rise *Nature Climate Change* **6** 777–80
Weeks J H and Harrison B J 2020 *Review of sea level rise science, information and services in Pakistan, Technical Report* Met Office (https://metoffice.gov.uk/binaries/content/assets/metofficegovuk/pdf/business/international/review-of-sea-level-rise-literature-for-pakistan—arrcc-report—external.pdf)
Zarfl C *et al* 2015 A global boom in hydropower dam construction *Aquatic Sciences* **77** 161–70